applied sciences

MDPI

Article

An Updated Earthquake Catalogue in Crete Derived by the Development of Local 1D Velocity Models and Hypocentre Relocation

Andreas Karakonstantis [1] and Filippos Vallianatos [1,2,*]

[1] Institute of Physics of the Earth's Interior and Geohazards, UNESCO Chair on Solid Earth Physics and Geohazards Risk Reduction, Hellenic Mediterranean University Research Center (HMURC), 73133 Chania, Crete, Greece; akarakon@geol.uoa.gr
[2] Section of Geophysics–Geothermy, Department of Geology and Geoenvironment, National and Kapodistrian University of Athens, 15784 Athens, Greece
* Correspondence: fvallian@geol.uoa.gr

Abstract: Crete is located in the Southern Aegean, in the southernmost part of the Hellenic Trench. Given the large number of earthquakes in the region generated by the convergence of the Eurasian and African tectonic plates, the research area is critical. More than 7000 manually revised events from 2018 to 2023 were used in this work to construct local 1D velocity models of Crete and the neighbouring areas. The P-wave velocity models were constructed using the spatiotemporal error minimisation method estimated using the HYPOINVERSE algorithm. At the same time, the V_P/V_S ratio was obtained using the Chatelain method, which compares the time difference in P and S phases recorded by pairs of corresponding stations. We then relocated the seismicity of the study area that was recorded by both permanent and temporary seismic networks during the abovementioned period. The double-difference algorithm was used to relocate events with magnitudes above the magnitude of completeness, resulting in more than 4500 precise relative locations with horizontal and vertical uncertainties of less than 2.5 km. The precise locations delineated faults both on the island and in the offshore study area. Furthermore, the results are discussed and compared with the ones derived from other significant previous works presented recently. The final dataset analysis contributes to a better understanding of the research area's seismicity as triggered by local and regional tectonic structures.

Keywords: velocity models; local tectonics; Hellenic Trench; relocation; Crete

Citation: Karakonstantis, A.; Vallianatos, F. An Updated Earthquake Catalogue in Crete Derived by the Development of Local 1D Velocity Models and Hypocentre Relocation. *Appl. Sci.* **2023**, *13*, 9860. https://doi.org/10.3390/app13179860

Academic Editors: Mimmo Palano, José A. Peláez and Carlos Marin-Lechado

Received: 31 July 2023
Revised: 26 August 2023
Accepted: 28 August 2023
Published: 31 August 2023

1. Introduction

Greece, located in southeastern Europe, is a place where a variety of geological processes take place, such as the formation of the Alpine mountain chain from the Western French Alps to the Dinarides in the Balkan Peninsula due to the collision between the European and Nubian plates [1–4]. In the Southern Aegean (Greece) lies the southernmost segment of the Hellenic Arc, which starts in the W-SW region of the Peloponnese, then continues south of Crete, splitting into three main parts, the Pliny, Ptolemy, and Strabo trenches, and terminates east of Rhodes Island before its differentiation into Anatolia and the South of Cyprus [5,6]. This region is characterized by intense rates of seismicity resulting from the convergence of the Eurasian and African tectonic plates, as shown by significant historical activity [7]. The aforementioned motions are driven by the subduction of the Mediterranean lithosphere of oceanic origin under the Aegean continental one, with a rate of convergence of ~35 mm/year [6–12].

This study focuses on the island of Crete, located at the southernmost tip of the Southern Aegean at the centre of the Hellenic Arc (Figure 1). This area appears to be one of the most seismically active areas in the eastern Mediterranean region, mainly due to intense tectonic movements during the Late Quaternary, which led to a significant uplift

in local scale and the creation of extensional faults in approximately the WNW–ESE and NNE–SSW directions [3,13–15]. In the Cretan Sea, north of Crete, three primary tectonic depressions are present, located between the Southern Cyclades and Crete, Karpathos, and Rhodes. The main tectonic structures in the region are oriented NW-SE to the west and NE-SW to the east, illustrating the curvature of the Hellenic Arc. The broader area of Crete is characterised by complex geodynamics where transpressional tectonics dominate the southern part of Crete, in contrast to normal and strike-slip forms on the shallow part of the crust, producing a heterogeneous stress field [16,17]. In contrast, in the north, the area between Santorini and Crete, extension is observed [18–21]. The latter shows extension in a general E-W direction, while N-forward shortening was observed in Western Crete [22]. Specifically, the faults in the area of Western Crete are divided into six categories, according to [23], whose directions are: (a) N130° E, (b) N100° E, (c) N020° E, (d) N075° E, (e) N050° E, and (f) N160° E. Ref. [6] determined that of the fault categories mentioned above, we find mainly normal faults (a–d), while (e) and (f) refer to strike-slip faulting, with sinistral and dextral motion of the slip components, respectively. On the contrary, in Central and Eastern Crete, extension is observed in the NE-SW and NW-SE directions as [24] mentioned.

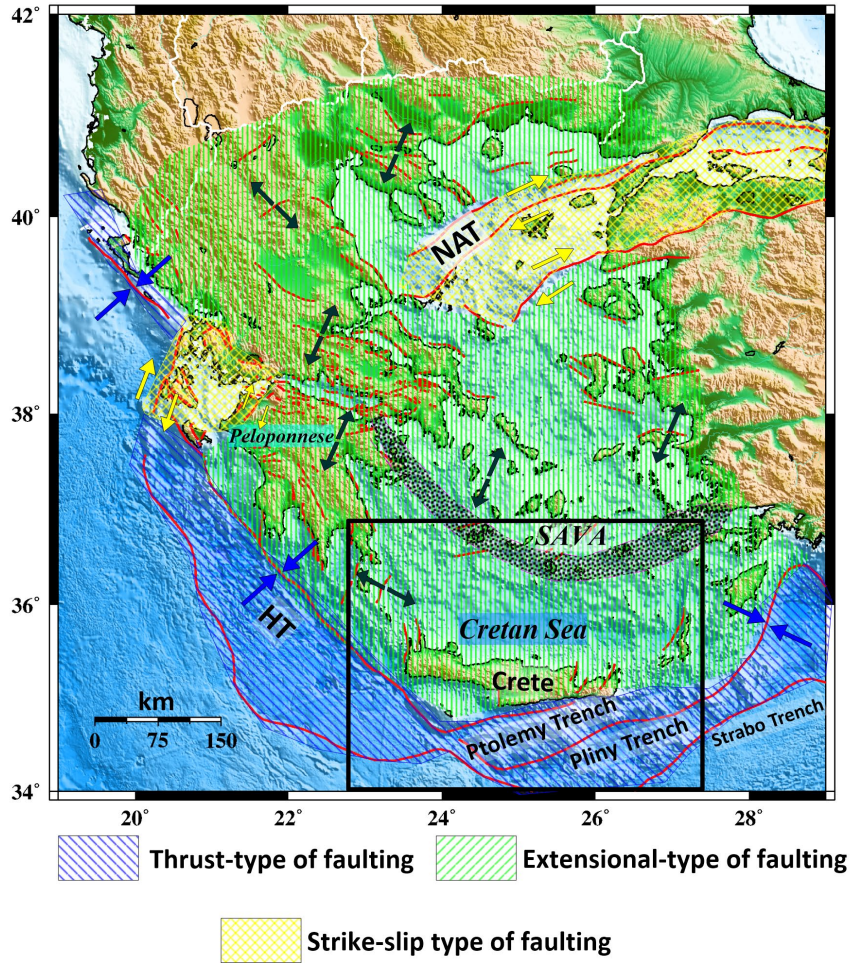

Figure 1. Main tectonic features in Greece and Western Turkey. The black rectangle contains the study area. Abbreviations-HT: Hellenic Trench; NAT: North Aegean Trough; SAVA: South Aegean Volcanic Arc. Fault traces (red lines) derived by [3,13]. Blue and green arrows indicate trend of the major (S1) and minor (S3) principal stress axes, yellow arrows show the strike-slip motion on the projected faults [16].

Crete's seismicity, in both the historical and instrumental periods, is mainly related to the geodynamics of the Aegean and Mediterranean plate convergence, and events of shallow depth characterise it (<25 km) [7,25–28]. The lack of uniform and optimal coverage with seismic stations on the island and local velocity models is a significant disadvantage in highlighting the earthquake distribution in areas near or along the HT. The latest essential sequences led to an amelioration of the local station coverage, improving the available catalogues. Improved 1D regional models and well-localised aftershocks recorded by dense seismic monitoring networks provide a basis and baseline for more constrained seismic velocities in the region and detailed seismic catalogues. Since the usage of manually selected high-quality arrival times (P and S) in 2018, local 1D body-wave velocity models were developed in the regions of West, Central, South-Eastern (Ptolemy and Pliny Trenches), and Eastern Crete. The recorded data improved the knowledge of the seismotectonic structures on the island and helped ameliorate the local shallow crustal seismicity relocation in order to examine in detail the correlation between seismicity and the activation of the local fault pattern. The resulting information can be used in future work to determine the 3D body-wave velocity structure of the Southern Aegean in order to provide more details on seismogenic layer thickness and the depth of the upper layers of the slab and assess the potential seismic hazard.

2. Materials and Methods

2.1. Seismological Data

The present work focuses on the island of Crete and its neighbouring regions to the west and east, respectively. Several permanent stations of the Hellenic Unified Seismological Network (HUSN) are operating in this area, complemented by 4 temporary stations (CRE1–4) of the Geodynamics Institute of the National Observatory of Athens (GI-NOA), installed between 27 September 2021 and 15 June 2022, mainly contributing to increasing the depth accuracy of the Arkalochori aftershock sequence for this period of time [29–31] (Figure 2).

Each event is recorded by at least 6 stations. Since 2007, continuous waveform recordings have been obtained from HUSN in real time, comprising both 1-component (1 Hz) (THR2-9; Santorini Island Seismic Network operated by the Aristotle University of Thessaloniki) and 3-component (either broad-band or short-period) stations, while manual arrival-time picking is applied to obtain hypocentral locations using the SeisComP3 graphical user interface [32] and a custom regional 1D velocity model for the region of Crete [33]. In the first stage of the sequence analysis, hypocentres were located in near real-time, employing the Hypo71 single-event algorithm [34]. Then they were relocated running the HypoInverse code (35-Klein, 2002). The dataset comprises 11,337 events from June 2018 to May 2023, with $M_L \geq 0.7$ (Figures 3 and 4), analysed and available in near-real time by the Seismological Laboratory of the National and Kapodistrian Univerity of Athens (SL-NKUA; http://www.geophysics.geol.uoa.gr/stations/gmaps3/leaf_stations.php?map=2&lng=en, accessed on 1 June 2023).

2.2. Estimation of the Local 1D Velocity Models

During the first phase of this work, a manual revision of the P and S phases took place for more than 11000 seismic events with $M_L \geq 0.7$. The initial locations of the data used were located using the regional velocity model of [33] using Hypo71 and HypoInverse codes [34,35]. Further filtering of this catalogue was applied in order to have more accurately determined events in the database for the minimum 1D velocity model inversion using the mean travel-time residuals and location error (RMS, ERX, ERY, and ERZ) minimization method [36,37]. Afterwards, the dataset was filtered for earthquake magnitudes greater or equal than the magnitude of the completeness (Mc) for the study area as determined by [38] (Figure 5). The initial phase data were further filtered using earthquakes with at least eight (8) P- and five (5) S-wave arrival times and a maximum azimuthal gap of 180°. In total, we obtained a dataset of 7410 events.

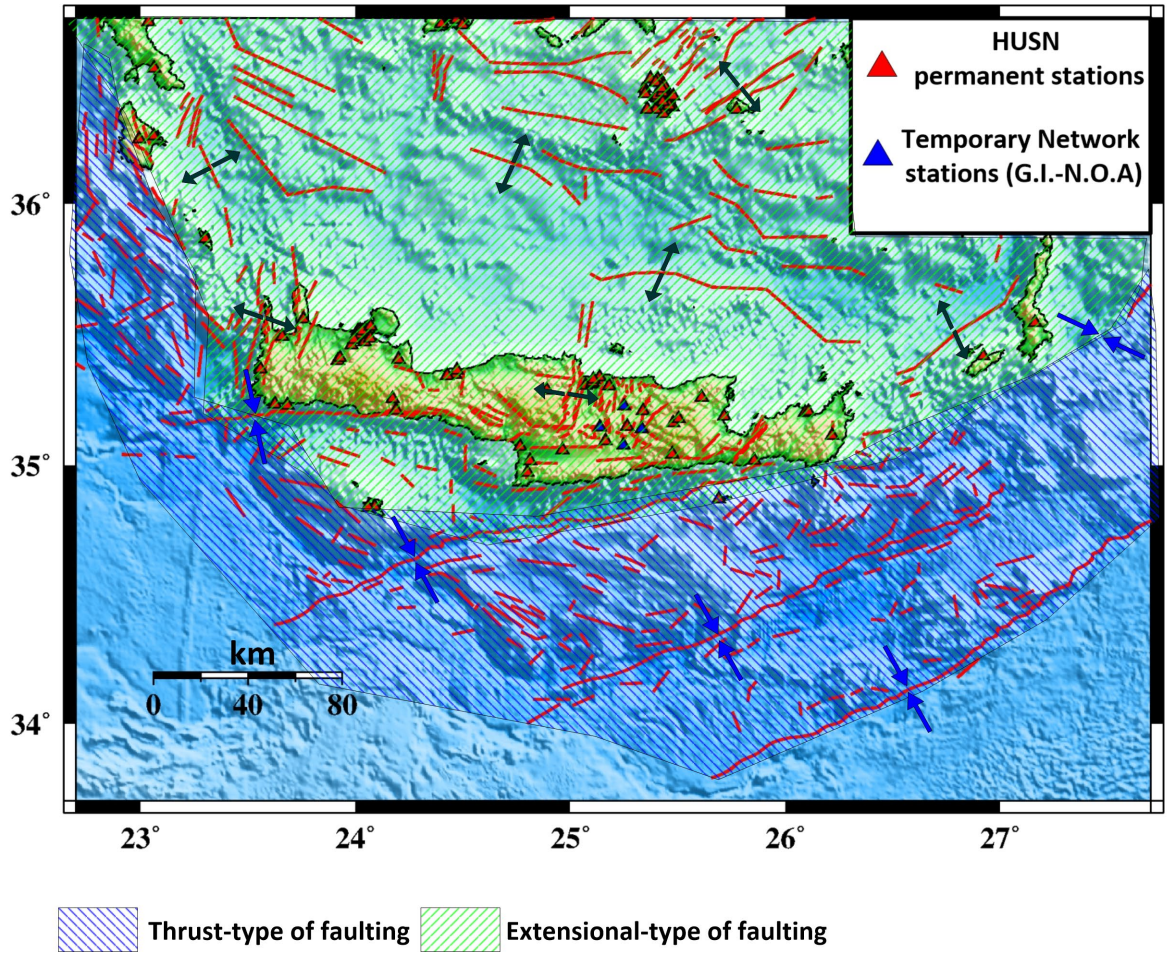

Figure 2. Location of the permanent (orange triangles) HUSN stations and temporary installed stations (blue triangles) by the G.I.-N.O.A after the initiation of Arkalochori earthquake sequence (September 27, 2021). Blue and green arrows indicate trend of the major (S1) and minor (S3) respectively [16].

The resulting catalogue was then divided spatially into six smaller regions (Figure 5) using overlapping windows for further analysis and comparison with similar studies conducted in these regions [39]. The events were evenly distributed across both overlapping areas. These areas are:

1. Chania-Antikythera region (area 1; 1882 events).
2. Rethymno area (area 2; 498 events).
3. Matala—Ptolemy Trench (area 3; 858 events).
4. Central Crete-Heraklion basin (area 4; 2321 events).
5. SE Crete—Pliny Trench region (area 5; 1096 events).
6. Zakros—Karpathos region (area 6; 1648 events), where the 12 October 2021, M_L = 6.2 event took place.

The largest group is that of Heraklion, which contains the aftershock sequence of Arkalochori [31,32,40,41]. A region-specific 1D velocity model was estimated for each group to further refine the initial hypocentral solutions in each area (Figure 5). The selected seismic phases were recorded by stations up to the distance of 200 km based on the Dmin-Dmax option provided by the HypoInverse code, targeting to exclude the Pn and Sn phases. Afterwards, a search for the best solution after multiple iterations per layer (velocity, ceiling depth), starting from the initial 1D velocity model. A gradual reconstruction of the final 1D velocity structure was performed based on evaluating a misfit function (RMS, ERH and ERZ) for a range of ceiling depth and velocity values. The robustness of each model was

tested by several HypoInverse runs, calculating the obtained error as a change in number and the ceiling depth of the layers.

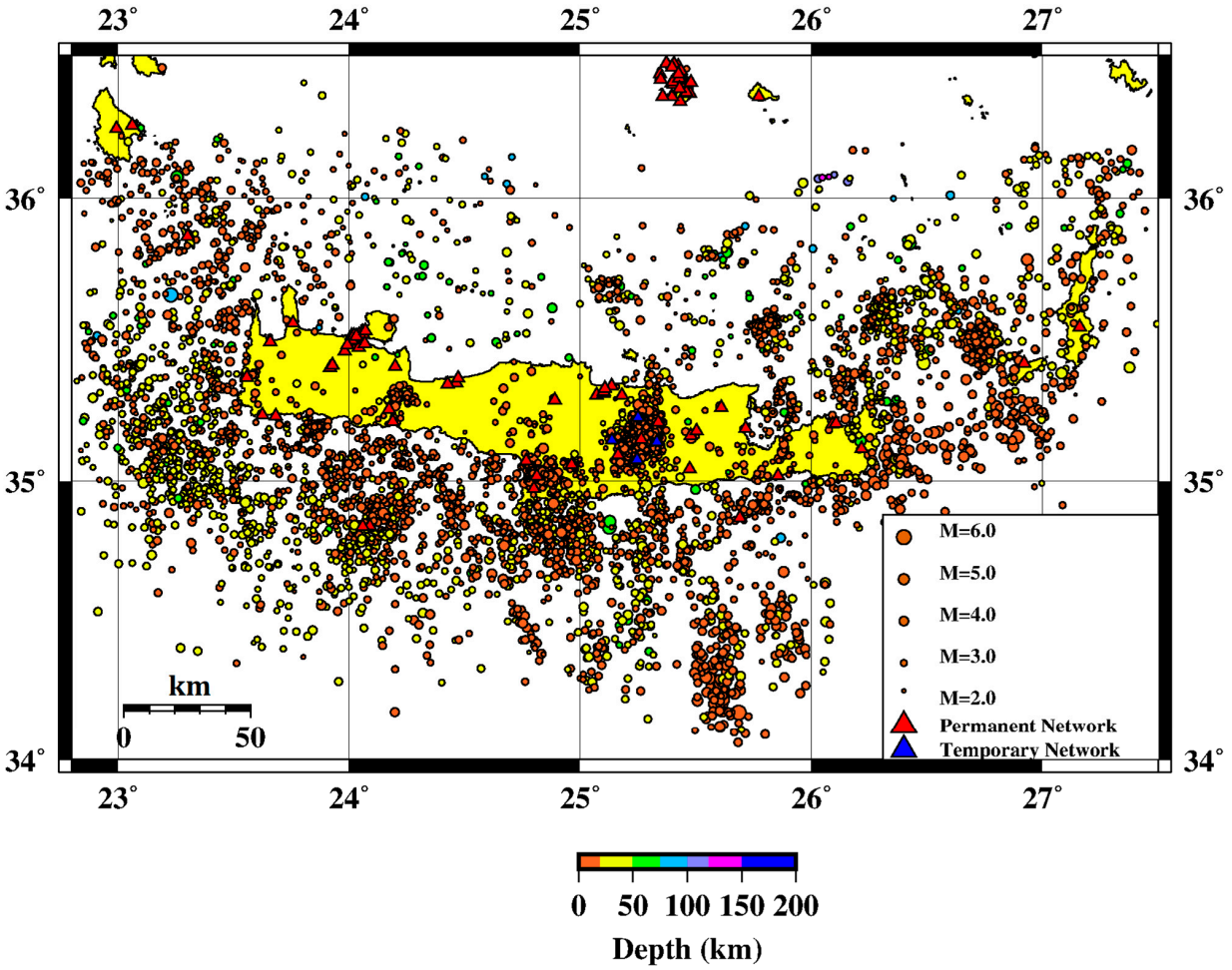

Figure 3. Spatial distribution of the initial 11,337 events ($M_L \geq 0.7$) from June 2018 to May 2023.

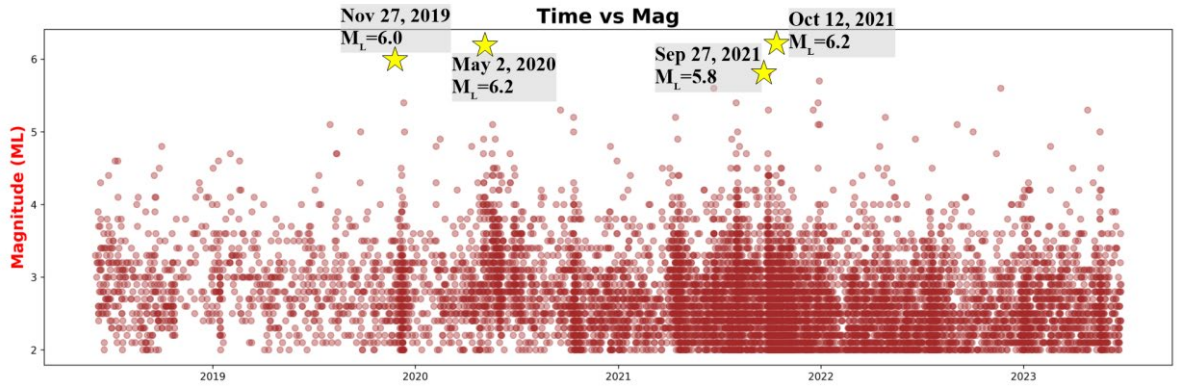

Figure 4. Magnitude (M_L)-time (years) of the $M_L \geq 2$ earthquake occurrences from June 2018 to May 2023.

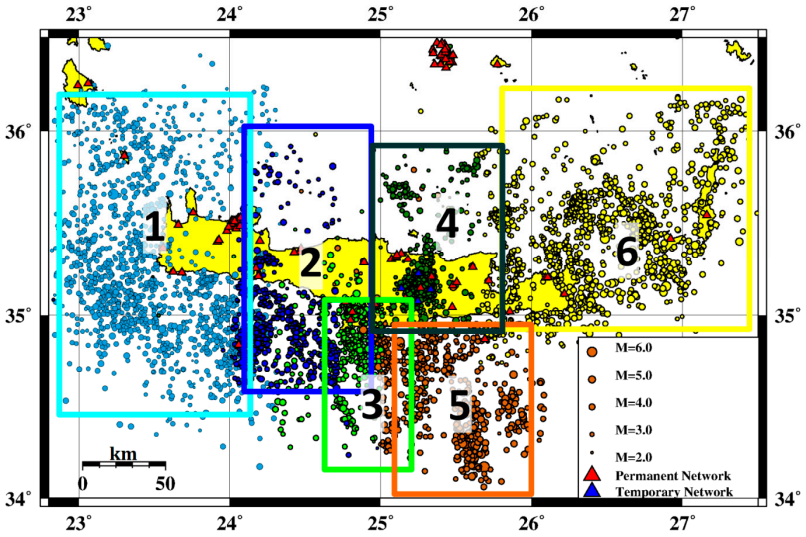

Figure 5. Spatial distribution of 7410 events with $M_L \geq 2.2$) from June 2018 to May 2023.

In each area, the procedure started with the estimation of hypocentral parameters using the local 1D velocity models obtained by [39]. The respective S-wave model was estimated by dividing the values of P-velocities to the V_P/V_S ratio obtained by the Chatelain method [42], which compares the time difference in P and S phases recorded by pairs of corresponding stations.

2.3. Double-Difference Algorithm (HypoDD)

The construction of a well-defined catalogue is essential to obtain a detailed image of the structural properties and processes that trigger seismic activity. The precision of hypocentre locations and their uncertainties depend on several factors, including the number and quality of available seismic phases, the accuracy with which arrival times are measured, the network geometry, and knowledge of the velocity structure and the linear approximation to a set of non-linear equations, which is assumed in the inversion. HypoDD ([43]; Waldhauser) is an algorithm that reduces the residuals between the observed and theoretical differences of travel times (or double-differences) for pairs of neighbouring events at each station that recorded both events, as can be seen from Equation (1). This way, errors due to unmodeled velocity structures are minimised without station corrections. A minimum 1D layered velocity model was used to predict the travel time differences and partial derivatives (Equation (2)).

$$dr_k^{ij} = (t_k^i - t_k^j)^{obs} - (t_k^i - t_k^j)^{cal} \quad (1)$$

$$\frac{\partial t_k^i}{\partial m}\Delta m^i - \frac{\partial t_k^i}{\partial m}\Delta m^j = dr_k^{ij} \quad \text{where } m = (x, y, z) \quad (2)$$

Inter-event distance and misfit weighting was applied to catalogue data after the end of each iteration in order to optimise their quality during the relocation procedure. Horizontal and vertical relative spatial errors can be minimized by approximately one order of magnitude under certain conditions. In this case study, the relocation took place in each sub-region that was described in the previous section. The initial phase data were further filtered using earthquakes with at least eight (8) P- and five (5) S-wave arrival times and a maximum azimuthal gap of 180°, resulting in 4609 events with $M_L \geq 2.2$. Initially, the events were located using hypoDD. Later, 4107 of them (89.11%) were relocated. A different approach of defying "strong links" was adopted throughout the sub-regions where the relocation procedure took place (Figure 6). The main factors that were taken into account were the size of the dominant clusters, the network coverage of the area, and the occurrence

of an aftershock sequence that could reduce the maximum separation distance in the ph2dt input parameter file.

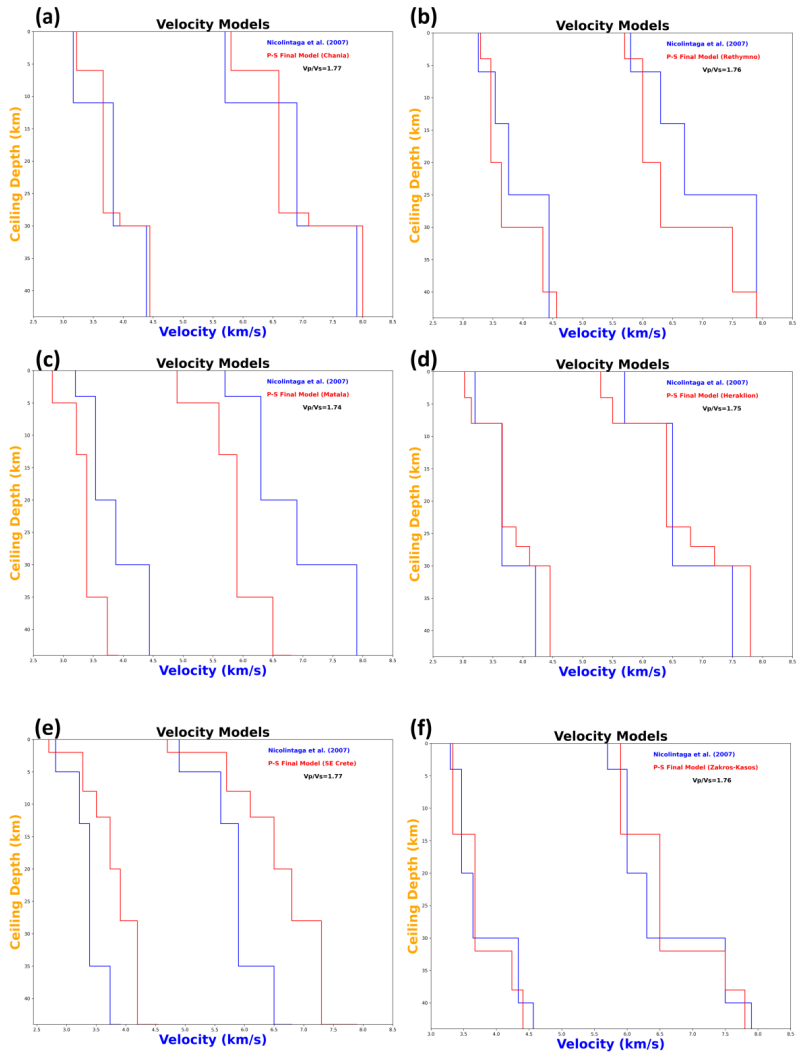

Figure 6. Initial [39] and final velocity models of V_P and V_S determined by the mean travel-time residuals for the areas of (**a**) Chania-Antikythera, (**b**) Rethymno, (**c**) Matala, (**d**) Central Crete, (**e**) SE Crete-Pliny Trench, and (**f**) Zakros-Karpathos.

3. Results

3.1. Local 1D Velocity Models and Location of the Seismic Catalogue

Taking into account the final residuals, a 1D P-wave velocity model ("P-S final model"; Figures 6 and 7) was determined. The distribution of the spatio-temporal errors obtained using the newly developed local velocity models is shown in Table 1. The horizontal and vertical shift of the hypocentres, which arose between the initial and final regional velocity model, is shown in the supplementary material. The majority of events in the final seismic catalogue lie between 2 and 16 km in depth. The shallow seismicity is distributed along the faults that intersect the shallow part of the crust [13], while a significant portion of intermediate-depth seismic activity ($H \geq 40$ km) is located near Antikythera Island (West; sub-area 1 in Figure 5), north of Heraklion (central part; sub-area 4 in Figure 6d), and between Eastern Crete and the Kassos and Karpathos Islands (East; sub-area 6 in Figure 5). This observation shows a fair correlation between the rapid increase in velocity at depths greater than 32 km in these areas (Figure 6f) and recent tomographic studies in the regions along the Hellenic Arc. [44–51].

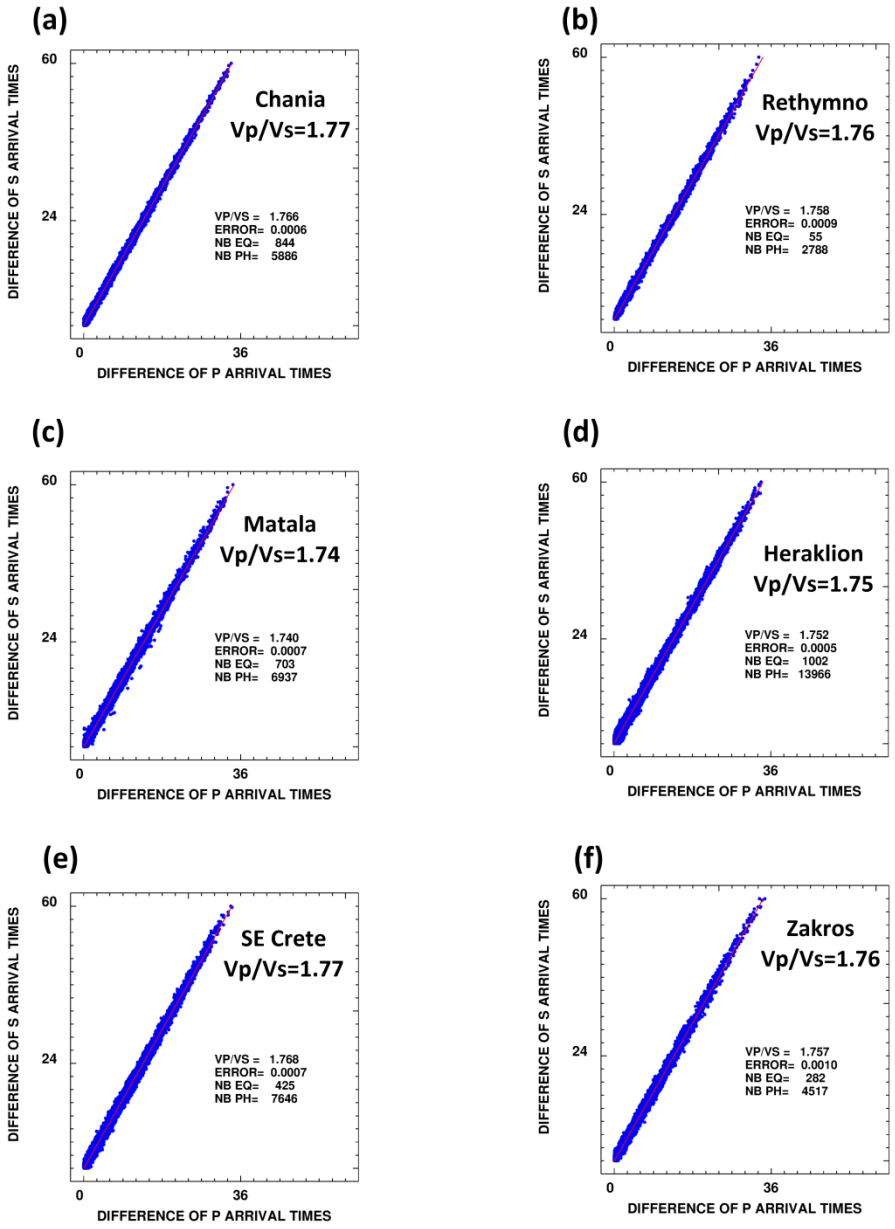

Figure 7. V_P/V_S ratio obtained using the Chatelain method [42] in the areas of (**a**) Chania, (**b**) Rethymno, (**c**) Matala, (**d**) Central Crete, (**e**) SE Crete-Pliny Trench, and (**f**) Zakros-Karpathos.

Table 1. Statistics of temporal errors (RMS), location uncertainties and mean depth for Crete's regional and group-specific initial [39] and final velocity models derived by this study.

Model	Regional Model [33]	Area 1	Area 1 [39]	Area 2	Area 2 [39]	Area 3	Area 3 [39]	Area 4	Area 4 [39]	Area 5	Area 5 [39]	Area 6	Area 6 [39]
RMS (s)	0.48	0.39	0.42	0.27	0.34	0.18	0.20	0.24	0.25	0.27	0.25	0.29	0.24
ERH (km)	1.44	1.95	2.27	1.68	2.47	1.90	2.37	1.74	2.10	1.61	2.36	1.71	2.21
ERZ (km)	4.74	6.90	7.25	4.58	7.25	4.99	9.08	5.62	6.36	6.59	15.08	6.02	5.45
Mean Depth (km)	33.70	17.22	13.69	15.82	11.88	11.34	11.01	8.07	13.69	10.70	9.12	15.69	15.49

The best 1D local velocity models are displayed. Their error statistics are shown in both histogram and map projection in Figures S1–S12. The histograms depict the temporal (RMS) and spatial (ERH and ERZ) error distributions of the available data between the study's starting [39] and final models. The newly developed velocity models provide us

with a better concentration of seismic events, more realistic hypocentre depth ranges, and a proper understanding of local structure activation.

In the westernmost region (Antikythera-Chania), the velocity model of the crust varies between 5.8 and 6.7 km/s for approximately 32 km, while the respective values for the neighbouring area of Rethymno are between 5.6 and 6.8 km/s for crustal thickness of less than 31 km (Figure 6b). The structure is relatively simplified since they are composed of four and three layers, respectively. Ref. [52] shows a more detailed image of the upper crust using data from seismic surveys conducted in the area. Their P-wave velocity model is composed of four (4) layers in the uppermost 2 km and reaches 5.2–5.3 km/s below 4 km of depth.

Moving to the SE, in the region of Matala-Central Ptolemy Trench (sub-region 3), significant differentiation is observed in the velocity structure of the crust compared to the one calculated by [39]. More specifically, the final model consists of five layers and a half-space at the same depths as the study by [39], with the noticeable difference situated in the P wave velocities and a significantly lower V_P/V_S ratio. The velocity model of the crust varies between 4.9 and 6.8 km/s for approximately 25 km, while the respective values for the neighbouring area of Rethymno are between 5.6 and 6.8 km/s for crustal thickness of less than 31 km (Figure 6b,c). The velocity model of Matala-Central Ptolemy Trench was tested in the recent earthquake sequence near Matala (17 May 2023–31 May 2023), where more than 130 events were located with a better concentration near some of the most significant local fault sources [13,52] and yielded improved error uncertainties compared to the initial model of [39].

In the central part of the island, the velocity model is divided into more layers (six layers) with approximately the same values of P velocity and crustal thickness. However, the V_P/V_S ratio changes from Rethymno (1.76) to Matala (1.74) and Heraklion (1.75) area (Figure 7b–d). The existence of a thick layer of recent deposits (Neogene to Quaternary) above the Alpine basement and the presence of a low-angle subducting lithosphere in the area may explain the reason of the complexity of the local velocity. Our results show a fair correlation with the ones of [53] for the uppermost (<10 km) part of the crust. Precisely, that study estimated a P-wave velocity between 4.8 and 5.5 km/s.

Further to the east, in the sub-regions of SE Crete-Pliny Trench and Zakros-Karpathos, the velocity model is simplified to approximately four (4) layers and a crustal thickness of 32–33 km (Figure 6e,f) due to the absence of clear minima during the process of defining the velocity and ceiling depth of the half-space. This result converges with the respective ones of [39,48] for the same territory in quantity, ceiling depth of the discontinuities ($\pm$2 km), and the velocity of each layer ($\pm$0.2 km/s). The updated catalogue shows a better concentration of shallow seismic events along the main fault zones of the study area (Figures S1–S12) and minor spatio-temporal errors (Table 1). The higher V_P/V_S ratios of the South Cretan Sea (sub-region 5; 1.77) and Eastern Crete-Karpathos Island (1.76) than the respective ones in sub-gions 3 and 4 may reflect the effect of the upward migration of fluids as a result of the dehydration of the subducting sediments within the oceanic origin Tethys plate [54–58], like in comparable cases [59–62]. Specifically, this V_P/V_S increase may be attributed either to the penetration of water fluids through local faults and flat cracks, saturating the hosting rock formation, or an upward migration of aqueous fluids derived by slab dehydration in the deeper parts of the crust (>10 km), circulating along the main fault zones of the area, fitting most of the observations on local seismic activity and previous studies of earthquake tomography in the region [45]. The subduction of the Tethys oceanic lithosphere under the Aegean microplate causes overlapping velocities, as shown in studies using earthquake, seismic, and gravity data [1,39,46,48,49,53]. This overlapping makes it challenging to create local 1D velocity models for each plate separately.

3.2. Relative Locations (hypoDD) of the Seismic Catalogue

In this study, more than 4500 events of $M_L \geq 2.2$, comprising 69,201 phases, were relocated with hypoDD (Figure S13). The procedure of the relative hypocentral relocation was performed for each sub-region (1–6) separately, using the local velocity models and

V_P/V_S ratio described in the previous section. Due to the size and the large number of seismic events in each area, the hypoDD relative locations were estimated using the LSQR method, which may under-estimate the respective errors.

The damping parameter for each area was set to different values in order to produce condition numbers between 40 and 80 for relocated clusters as suggested by [43]. A total of 4113 events were successfully relocated (~89%) with an average RMS residual of 0.18 s, which is significantly lower than the respective one of the absolute locations obtained with HYPOINVERSE, which is 0.30 s. The lack of fidelity in these error estimations led us to divide the data into even smaller clusters in order to produce more accurate location uncertainties using the singular value decomposition (SVD) method [43]. Then, the catalogue was merged and the average obtained uncertainties for each sub-region are shown in Table 2. In Figures 8 and 9, the displacement between the epicentre locations obtained using the single-event (HYPOINVERSE) and the double-difference (hypoDD) algorithms as well as the depth distribution between the initial and the final catalogue is shown in both map projection and histogram graph.

Table 2. Statistics of spatial errors and centroid coordinates and depth for each sub-region using the SVD method to assess the relative relocation uncertainties.

Area ID	Total Number of Earthquakes (Sum of Smaller Clusters)	Centroid Lat (°N)	Centroid Lon (°E)	Centroid Depth (km)	ErrX (km)	ErrY (km)	ErrZ (km)
1	652	35.57	23.48	7.49	2.2	2.5	4.8
2	578	34.98	24.05	11.46	0.7	0.8	0.9
3	110	35.02	24.83	5.53	1.8	0.6	1.2
4	1974	35.15	25.26	10.35	0.5	0.8	1.0
5	615	34.71	25.36	18.02	2.2	1.0	3.6
6	799	35.58	26.31	21.37	0.5	1.6	2.0

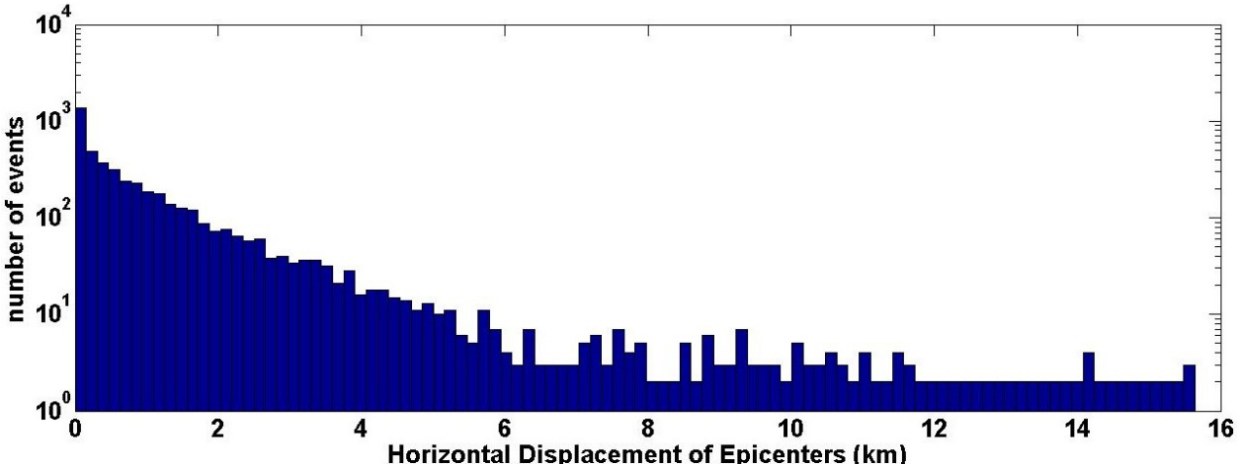

Figure 8. Histogram of the absolute frequency (log scale) of the displacement between the located and the relocated events in km.

In the westernmost region (Antikythera-Chania), 652 out of 683 events of the initial locations ($M \geq 2.2$) were relocated with HYPODD, giving a first result that could be rated as satisfactory. The calculation of differential travel times resulted in an average number of seven links per event pair and an average offset between the linked events of 3.37 km. There were approximately 29% weakly linked events and 0.5% strongly linked events. The relocated seismic events (supplementary material) are mainly concentrated in the N-S striking normal faults west of Kissamos gulf, and some smaller clusters are located south of Crete, along the HT, or near Kythera-Antikythera in greater depths ($H \geq 30$ km).

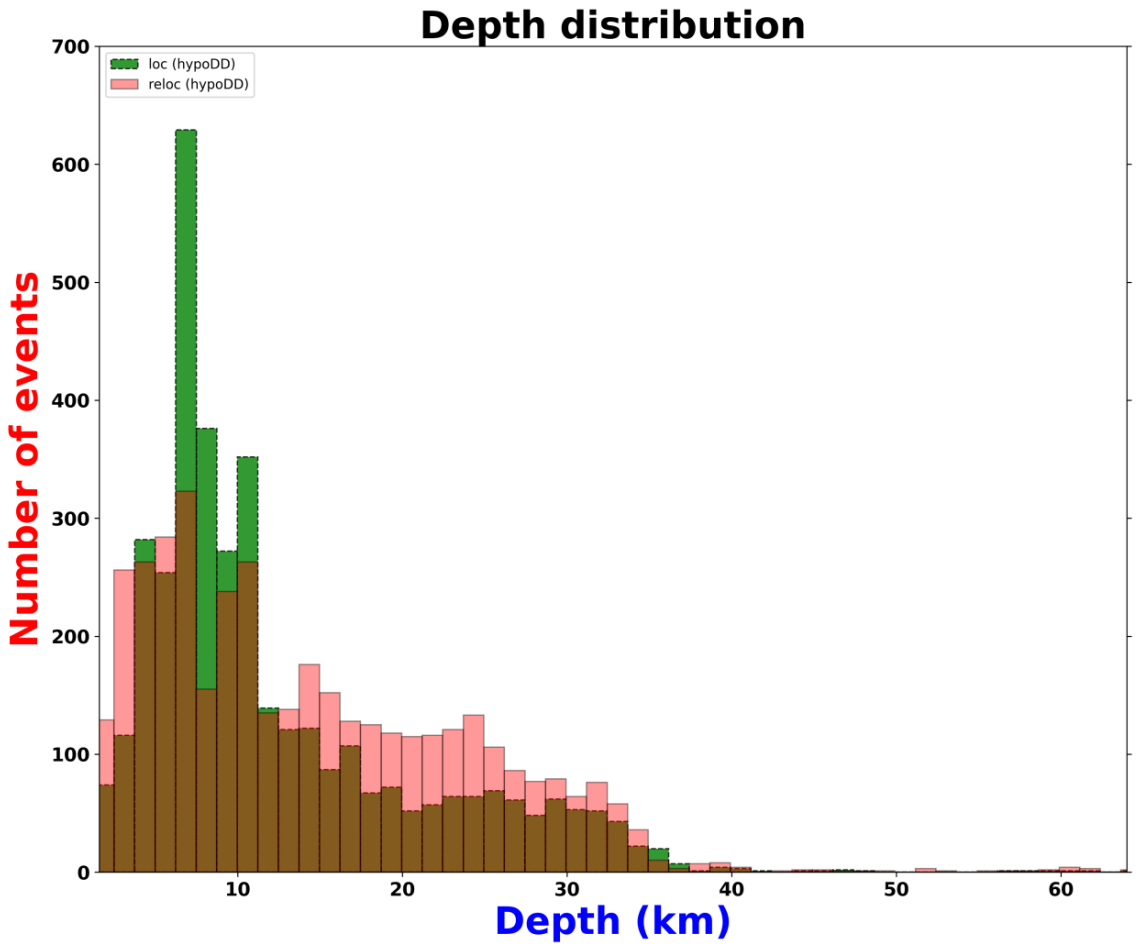

Figure 9. Histogram of the depth distribution of the relocated catalogue.

In the area of Rethymno (sub-region 2), 578 out of 656 events of the initial catalogue ($M \geq 2.2$) were relocated with hypoDD, improving the concentration of the earthquakes along main faults. The calculation of differential travel times resulted in an average number of seven links per event pair and an average offset between linked events of 2.93 km. The earthquakes of the relocated catalogue are mainly concentrated in the E-W striking thrust offshore faults south of Crete, and some sparser clusters, related to the activity of the HT, are located in the area ~30 km SSW of Crete, in the vicinity of Gavdos Island (supplementary material).

In area 3 (Matala), most of the events that were relocated using hypoDD belong to the earthquake sequence that occurred near Matala between 17 May 2023 and 31 May 2023. More than 130 events were located using the local velocity model obtained using the data of this study, achieving a better concentration near some of the most significant local fault sources [13,52] as a first result. The calculation of differential travel times resulted in an average number of five links per event pair and average offset between linked events of 2.07 km. The earthquakes of the relocated catalogue are mainly concentrated in between the E-W striking, north (Siva fault) and south (Gortyna fault) dipping normal faults 2 km east of Matala (supplementary material).

The majority of the events of sub-region 4 (Heraklion, Central Crete) belong to the 2021–2022 Arkalochori earthquake sequence. The 27 September 2021 mainshock (Mw = 6.0) was preceded by 300 events of $M_L \geq 2.2$ in the area between the Galatas and Avli normal faults in the area S-SE of Heraklion city. The epicentre of the mainshock was located less than 5 km to the SE of Arkalochori (lat: 35.1433° N, long: 25.2688° E) at a depth of ~9.5 km, slightly different from that of [63–65]. The denser cluster of events is located

west of the mainshock in an approximately 15 km long area associated with the foreshocks (June–September 2021). A significant cluster can be seen in the region between the Amourgeles and Parthenio N-S striking normal faults, while to the NE, a major group of events is concentrated in the footwall of the Agnos NE-SW-oriented normal fault near the town of Kastelli (supplementary material). The majority of the focal depths are between 4 and 16 km.

In the area of SE Crete-Pliny Trench (sub-region 5), the results show small (or no) improvement in the relocation process due to the greater distance of the nearest station and the large azimuthal gap of the initial location data. Most seismic events of the initial catalogue are concentrated in clusters along the Cretan and the Pliny Trench south of Crete. In this application, a significant portion of the initially located seismic catalogue is eliminated from the relocated data due to the absence of nearby stations.

In the area of Zakros-Karpathos (sub-region 6), 799 out of 832 events of the initial catalogue ($M \geq 2.2$) were relocated with hypoDD, improving the concentration of the earthquakes along the main local and regional fault zones (supplementary material). The calculation of differential travel times resulted in an average number of eight links per event pair and average offset between linked events of 2.39 km. Seismicity was divided into some smaller clusters that are characterised by a range of hypocentral depth. Specifically, earthquakes of intermediate depth ($32 \leq H(km) \leq 50$) are detected both in Karpathos (~10 km N of Kasos), east and north of Agios Nikolaos, and in the Cretan Sea to the north (~50 km NNE of Agios Nikolaos). Accordingly, surface earthquakes are located near the fault that defines the eastern end of Mirabello Gulf and Sitia (~20 km NNW of Zakros), with depths ranging from 3.5–21 km.

Furthermore, six (6) cross-sections were performed in order to see the impact of the relocation procedure on the sequence hypocentral depths and the discrimination of the local activated structures (Figure 10). Cross-sections 1-2 (A-A′, B-B′) have an E-W and NNE-SSW orientation, respectively. Cross-section A-A′ covers the study areas from Antikythera to Karpathos Island in an E-W direction, cutting the main N-S striking offshore normal faults of the Cretan Sea. In this section, the dip angle differs from one corner of the study area to the other. In the regions of Chania and Rethymno, the local faults appear to have a low angle, while at depths greater than 30 km, a low-angle surface is evident in the first 75–80 km of the cross-section, possibly related to the top of the subducted lithosphere in the area (Figure 11).

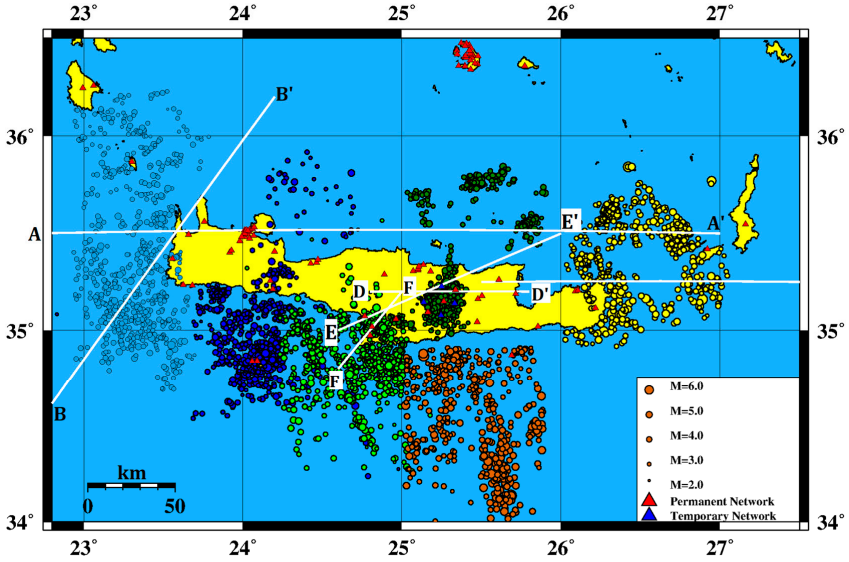

Figure 10. Presentation of the map of the 6 cross-sections, 5 km wide (A-A′, B-B′, C-C′, D-D′, E-E′ and F-F′). Different colours are the same as those in Figure 6.

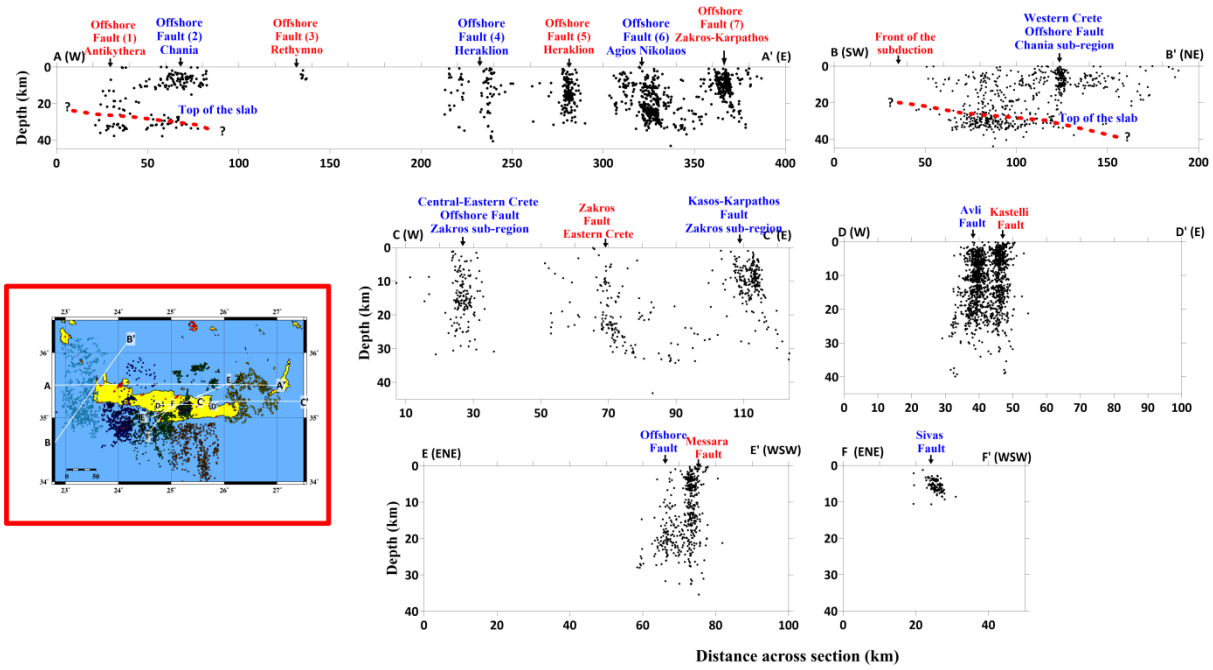

Figure 11. Depth cross-sections corresponding to the profiles shown in Figure 10. Black dots represent hypocentres of the relocated earthquakes in the broader study area. Projections of the nearest toponyms, fault zones, and moderate ruptures are shown at the top of each section.

This feature becomes more evident in the cross-section B-B′ that cuts vertically to the HT. This cluster becomes denser in the area that previous studies connected to the activation of a large segment of the HT and the occurrence of the famous tsunamigenic earthquake of 365 in Crete [7,13,25,27,40]. Cross-section C-C′ cuts the eastern part of Crete, from Agios Nikolaos to the area south of Karpathos island. The geometry of the hypocentres as they appear in the performed cross-section reveals the activation of some faults, dipping ~80° to the W, in the 2021–2022 Arkalochori seismic sequence area and two smaller ones, in the area between Agios Nikolaos and Zakros, related to the N-S striking high-angle normal faults. Cross-section D-D′ cuts the central part of the 2021–2022 Arkalochori aftershock sequence volume. In this section and in the respective one of D-D′, we can see two sub-vertical structures whose surface projection coincides with the Avli (~35 km in D-D′) and Kastelli (~45 km in D-D′) normal faults. A smaller cluster of earthquakes is observed in the sections E-E′ and F-F′ in the area SW of Crete Island, coinciding with sub-region 3 (Matala; Figure 11). The relocated hypocentres of these earthquakes are distributed from shallow depth down to about 25 km, possibly related to the Messara fault (E-E′), and a more shallow one (<10 km) connected to the Matala aftershock sequence near the Sivas north-dipping normal fault (F-F′).

4. Summary—Conclusions

This study examined seismicity in the region of Crete and neighbouring areas recorded by stations of HUSN from June 2018 until the end of May 2023 [66–69]. This included crustal earthquakes on the island and moderate events that occurred both onshore in local faults and offshore on the HT. These events were used to obtain local 1D velocity models using the mean travel-time residuals and location error minimization technique. Based on these models and the calculated travel times, a new catalogue of seismic events with well-constrained hypocentral parameters was compiled. In the next stage, this catalogue served as input data in order to ameliorate the absolute and relative locations with hypoDD. Both local and regional active faults in the area were highlighted with new results in our effort to obtain a more detailed image of the activated fault structures onshore and offshore of the island of Crete.

The newly developed velocity models in this research share several characteristics with those developed by [28,33,39,64]. The primary difference is that the models of [39,64] produced substantially shallower events than the events that belong in the Arkalochori seismic sequence in Central Crete [63]. In particular, the stronger events of that sequence (Mw = 6.0 and Mw = 5.3) were located at very shallow depths (H < 5 km), which looks improbable in terms of earthquake physics and the area's history [65–67]. The local 1D models in the first two areas west of the study area (Antikythera-Chania, Rethymno) have a relatively simplified structure since they are composed of four and three layers, respectively. Ref. [53] showed a more detailed image of the upper crust using data from seismic surveys conducted in the area. Their P-wave velocity model is composed of four (4) layers in the uppermost 2 km and reaches 5.2–5.3 km/s below 4 km of depth. The existence of a thick layer of recent deposits (Neogene to Quaternary) above the Alpine basement of different ages and lithology and the top of the low-angle subducting lithosphere (Figure 11) may explain why the velocity structure in Central Crete is divided into numerous layers. Our results show a fair correlation with the ones of [53] for the uppermost (<10 km) part of the crust. Precisely, that study estimated a P-wave velocity between 4.8 and 5.5 km/s. The model developed in the eastern portion of the island suggests a simple layout with four (4) strata (Figure 6a). The V_P/V_S ratio of the 1D model developed in Western and Eastern Crete is higher (1.77) than those of Central and SE Crete (1.74 and 1.75), which could be related to the closer location of the intermediate depth events reflecting an upward migration of fluids resulting from the dehydration of subducting sediments within the oceanic origin Tethys plate like in comparable cases [54–62]. The subduction of the Tethys oceanic lithosphere under the Aegean microplate results in velocities from both plates overlapping, making it difficult to address each plate individually in local 1D velocity models.

The relocation procedure managed to improve the relative locations of the 2018–2023 seismic catalogue, which are concentrated in the vicinity of the main local and regional fault zones. The main N-S striking offshore normal faults of the Cretan Sea were highlighted in sub-regions 1 and 2. More specifically, a differentiation in the dip angle of the moderate-size local faults from one corner of the study area to the other becomes evident. In the regions of Chania and Rethymno, the local faults appear to have a low angle, while at depths greater than 30 km, a low-angle surface is evident in the first 50 km of the cross-sections that were performed, possibly related to the top of the subducted lithosphere in the area. Some smaller concentrations of earthquakes were observed in two of the sections performed in sub-region 3, SW of Crete Island (Matala; Figure 11). The relocated hypocentres of these earthquakes were distributed from shallow depth down to about 25 km, possibly related to the Messara fault, and a more shallow one (<10 km) connected to the Matala aftershock sequence near the Sivas north-dipping normal fault. Further to the east, the geometry of the hypocentres as they appear in the performed cross-sections in Central Crete revealed the activation of some high-angle normal faults, dipping ~80° to the W, in the 2021–2022 Arkalochori seismic sequence area. The cross-sections that cut the 2021–2022 Arkalochori aftershock sequence volume reveal two sub-vertical structures whose surface projection coincide with the Avli (~35 km in D-D′) and Kastelli (~45 km in D-D′) normal faults. Ref. [63] describes that during the main phase of this seismic sequence. Apparently, a large asperity of a west-dipping normal fault was broken and distributed stresses towards its northern and southern edges, triggering aftershocks mainly in two large groups, separated by a spatial gap, which could result in this complex image of epicentre distribution. In the region of Eastern Crete (sub-region 6), two smaller activated features were revealed in the area between Agios Nikolaos and Zakros, related to the N-S striking high-angle normal faults.

Summarising, we can state that a new database of seismic events with well-constrained hypocentral parameters was compiled based on the newly formed local velocity models. The resulting models of the crust and upper mantle are comparable on a both local and regional scale with previous studies that used data from the seismic activity of the Southern Aegean and previous seismic surveys conducted in the region [1,46,48,49,53]. These 1D

velocity models aimed to improve the hypocentre locations of the available dataset. The regional distribution of seismic activity shows:

- A complex shallow structure in Crete's central region mainly attributed to the dense pattern of neotectonic faults;
- A smoother and more continuous image in deeper slices (>40 km) where high V_P/V_S ratio (>1.82) distribution is observed.

This process will provide a foundation for future studies on the Wadati–Benioff zone geometry in the Southern Aegean, as well as the identification of fault zones related to historical events with limited information and the properties (variation of thickness) of the seismogenic layer.

Supplementary Materials: The following supporting information can be downloaded at: https://www.mdpi.com/article/10.3390/app13179860/s1, Figures S1–S12: Distribution of the seismic events using the final P-S velocity model in the sub-regions and plot of the absolute locations as a function of horizontal uncertainty or ERH (left) and vertical uncertainty or ERZ (right) as well as histograms of the error statistics between the initial (green) and the final 1D model (red) obtained in this study. Figure S13: (a) Location of the 2018–2023 catalogue for 5321 events, (b) relocated events using hypoDD. Figures S14–S18: Distribution of the located (left) and relocated events (right) that occurred between June 2018 and May 2023 in the selected areas.

Author Contributions: Conceptualisation, A.K.; methodology, A.K. and F.V.; software, A.K.; validation, A.K. and F.V.; formal analysis, A.K. and F.V.; investigation, A.K. and F.V.; resources, A.K. and F.V.; data curation, A.K. and F.V.; writing—original draft preparation, A.K.; writing—review and editing, A.K. and F.V.; visualisation, A.K.; supervision, A.K. All authors have read and agreed to the published version of the manuscript.

Funding: This research received no external funding.

Institutional Review Board Statement: The study did not require ethical approval.

Informed Consent Statement: Not applicable.

Data Availability Statement: All data products generated in this study (velocity models, earthquake catalogues) are available from the authors upon request.

Acknowledgments: We would like to thank the scientists, post-graduate students, and personnel who participated in the installation or maintenance of the stations belonging to the HUSN and assisted in the signal processing and manual location of the recorded seismicity, as well as the three reviewers for their creative comments and suggestions. We used data from the following seismic networks: HL (Institute of Geodynamics, National Observatory of Athens, https://doi.org/10.7914/SN/HL), HP (University of Patras, https://doi.org/10.7914/SN/HP), HT (Aristotle University of Thessaloniki, https://doi.org/10.7914/SN/HT), HA (National and Kapodistrian University of Athens, https://doi.org/10.7914/SN/HA), HC (Seismological Network of Crete, https://doi.org/10.7914/SN/HC), and the HI Institute of Engineering Seismology and Earthquake Engineering, https://doi.org/10.7914/SN/HI).

Conflicts of Interest: The authors declare no conflict of interest.

References

1. Delibasis, N.; Drakopoulos, J.K.; Fytrolakis, N.; Katsikatsos, G.; Makropoulos, K.C.; Zamani, A. Seismotectonic Investigation of the area of Crete Island. In Proceedings of the International Symposium on the Hellenic Arc and Trench (HEAT), Athens, Greece, 8–10 April 1981; Volume 1, pp. 121–138.
2. Drakopoulos, J.; Delibasis, N. The focal mechanism of earthquakes in the major area of Greece for the period 1947–1981. *Seismol. Lab. Univ. Athens Publ.* **1982**, *2*, 1–72.
3. Ganas, A.; Oikonomou, I.A.; Tsimi, C. NOAfaults: A digital database for active faults in Greece. *Bull. Geol. Soc. Greece* **2017**, *47*, 518–530. [CrossRef]
4. Kiratzi, A.; Benetatos, C.; Vallianatos, F. Seismic deformation derived from moment tensor summation: Application along the Hellenic Trench. In *Moment Tensor Solutions*; D'Amico, S., Ed.; Springer: Cham, Switzerland, 2018. [CrossRef]
5. McKenzie, D. Active tectonics of the Alpine-Himalayan belt: The Aegean Sea and surrounding regions. *Geophys. J. R. Astr. Soc.* **1978**, *55*, 217–254. [CrossRef]

6. Le Pichon, X.; Angelier, J. The Hellenic Arc and trench system: A key to the neotectonic evolution of the eastern Mediterranean area, 1979. *Tectonophysics* **1979**, *60*, 1–42. [CrossRef]
7. Papazachos, B.C.; Papazachou, C. *The Earthquakes of Greece*; Ziti Publishing: Thessaloniki, Greece, 2003; p. 286. (In Greek)
8. Jackson, J.A.; White, N.J. Normal faulting in the upper continental crust: Observations from regions of active extension. *J. Strucr. Geol.* **1989**, *11*, 15–36. [CrossRef]
9. Le Pichon, X.; Chamot-Rooke, N.; Lallemant, S. Geodetic determination of kinematics of central Greece with respect to Europe: Implications for eastern Mediterranean tectonics. *J. Geophys. Res.* **1995**, *100*, 12675–12690. [CrossRef]
10. McClusky, S.; Balassanian, S.; Barka, A.; Demir, C.; Ergintav, S.; Georgiev, I.; Gurkan, O.; Hamburger, M.; Hurst, K.; Kahle, H.; et al. Global Positioning System constraints on plate kinematics and dynamics in the eastern Mediterranean and Caucasus. *J. Geophys. Res.* **2000**, *105*, 5695–5719. [CrossRef]
11. Briole, P.; Ganas, A.; Elias, P.; Dimitrov, D. The GPS velocity field of the Aegean. New observations, contribution of the earthquakes, crustal blocks model. *Geophys. J. Int.* **2021**, *226*, 468–492. [CrossRef]
12. Reilinger, R.; McClusky, S.; Paradissis, D.; Ergintav, S.; Vernant, P. Geodetic constraints on the tectonic evolution of the Aegean region and strain accumulation along the Hellenic subduction zone. *Tectonophysics* **2010**, *488*, 22–30. [CrossRef]
13. Caputo, R.; Catalano, S.; Monaco, C.; Romagnoli, R.; Tortorici, G.; Tortorici, L. Active faulting on the island of Crete (Greece). *Geophys. J. Int.* **2010**, *183*, 111–126. [CrossRef]
14. Shaw, B.; Jackson, J. Earthquake mechanisms and active tectonics of the Hellenic subduction zone. *Geophys. J. Int.* **2010**, *181*, 966–984. [CrossRef]
15. Werner, V.; Baika, K.; Fischer, P.; Hadler, H.; Obrocki, L.; Willershäuser, T.; Tzigounaki, A.; Tsigkou, A.; Reicherter, K.; Papanikolaou, I.; et al. The sedimentary and geomorphological imprint of the AD 365 tsunami on the coasts of southwestern Crete (Greece)—Examples from Sougia and Palaiochora. *Quat. Int.* **2018**, *473*, 66–90. [CrossRef]
16. Kapetanidis, V.; Kassaras, I. Contemporary crustal stress of the Greek region deduced from earthquake focal mechanisms. *J. Geodyn.* **2019**, *123*, 55–82. [CrossRef]
17. Vassilakis, E.; Alexopoulos, J. Recognition of strike-slip faulting on the supra-detachment basin of Messara (central Crete Island) with remote sensing image interpretation techniques. In Proceedings of the 4th EARSeL Workshop on Remote Sensing and Geology, Mykonos, Greece, 24–25 May 2012; pp. 108–115.
18. Kokinou, E.; Moisidi, M.; Tsanaki, I.; Tsakalaki, E.; Tsiskaki, E.; Sarris, A.; Vallianatos, F. A seismotectonic study for the Heraklion basin in Crete (Southern Hellenic arc, Greece). *Int. J. Geol.* **2008**, *2*, 9–16.
19. Floyd, M.A.; Billiris, H.; Paradissis, D.; Veis, G.; Avallone, A.; Briole, P.; McClusky, S.; Nocquet, J.M.; Palamartchouk, K.; Parsons, B.; et al. A new velocity field for Greece: Implications for the kinematics and dynamics of the Aegean. *J. Geophys. Res.* **2010**, *115*, B10403. [CrossRef]
20. Kaviris, G.; Papadimitriou, P.; Kravvariti, P.; Kapetanidis, V.; Karakonstantis, A.; Voulgaris, N.; Makropoulos, K. A detailed seismic anisotropy study during the 2011–2012 unrest period in the Santorini Volcanic Complex. *Phys. Earth Planet. Inter.* **2015**, *238*, 51–88. [CrossRef]
21. Papadimitriou, P.; Kapetanidis, V.; Karakonstantis, A.; Kaviris, G.; Voulgaris, N.; Makropoulos, K. The Santorini Volcanic Complex: A detailed multi-parameter seismological approach with emphasis on the 2011–2012 unrest period. *J. Geodyn.* **2015**, *85*, 32–57. [CrossRef]
22. Hatzfeld, D.; Pedotti, G.; Hatzidimitriou, P.; Makropoulos, K. The strain pattern in the western Hellenic arc deduced from a microearthquake survey. *Geophys. J. Int.* **1990**, *101*, 181–202. [CrossRef]
23. Ten Veen, J.H.; Meijer, P.T. Late Miocene to recent tectonic evolution of Crete (Greece): Geological observations and model analysis. *Tectonophysics* **1998**, *298*, 191–208. [CrossRef]
24. Armijo, R.; Lyon-Caen, H.; Papanastassiou, D. East-west extension and Holocene normal-fault scarps in the Hellenic arc. *Geology* **1992**, *20*, 491–494. [CrossRef]
25. Papadopoulos, G.A. Earthquake sources and seismotectonics in the area of Crete. In *Minoan Earthquakes-Breaking the Myth through Interdisciplinarity*, 1st ed.; Jusseret, S., Sintubin, M., Eds.; Leuven University Press: Leuven, Belgium, 2017; pp. 165–190.
26. Papanastassiou, D.; Latoussakis, J.; Stavrakakis, G. A revised catalog of earthquakes in the broader area of Greece for the period 1950-2000 from IG-NOA, 2001. In Proceedings of the 9th Congress of the Geological Society of Greece, Athens, Greece, 24–28 September 2001.
27. Kiratzi, A.A.; Karakaisis, G.F.; Papadimitriou, E.E.; Papazachos, B.C. Seismic source-parameter relations for earthquakes in Greece. *Pure Appl. Geophys.* **1985**, *123*, 27–41.
28. Meier, T.; Rische, M.; Endrun, B.; Vafidis, A.; Harjes, H.-P. Seismicity of the Hellenic subduction zone in the area of western and central Crete observed by temporary local seismic networks. *Tectonophysics* **2004**, *383*, 149–169.
29. Evangelidis, C.P.; Triantafyllis, N.; Samios, M.; Boukouras, K.; Kontakos, K.; Ktenidou, O.-J.; Fountoulakis, I.; Kalogeras, I.; Melis, N.S.; Galanis, O.; et al. Seismic Waveform Data from Greece and Cyprus: Integration, Archival, and Open Access. *Seism. Res. Lett.* **2021**, *92*, 1672–1684.
30. Vassilakis, E.; Kaviris, G.; Kapetanidis, V.; Papageorgiou, E.; Foumelis, M.; Konsolaki, A.; Petrakis, S.; Evangelidis, C.P.; Alexopoulos, J.; Karastathis, V.; et al. The 27 September 2021 Earthquake in Central Crete (Greece)—Detailed Analysis of the Earthquake Sequence and Indications for Contemporary Arc-Parallel Extension to the Hellenic Arc. *Appl. Sci.* **2022**, *12*, 2815. [CrossRef]

31. Vallianatos, F.; Michas, G.; Hloupis, G.; Chatzopoulos, G. The Evolution of Preseismic Patterns Related to the Central Crete (Mw6.0) Strong Earthquake on 27 September 2021 Revealed by Multiresolution Wavelets and Natural Time Analysis. *Geosciences* **2022**, *12*, 33. [CrossRef]
32. Behr, Y.; Clinton, J.F.; Cauzzi, C.; Hauksson, E.; Jónsdóttir, K.; Marius, C.G.; Pinar, A.; Salichon, J.; Sokos, E. The Virtual Seismologist in SeisComP3: A New Implementation Strategy for Earthquake Early Warning Algorithms Seism. *Res. Let.* **2016**, *87*, 363–373.
33. Becker, D.; Meier, T.; Bohnhoff, M.; Harjes, H.P. Seismicity at the convergent plate boundary offshore Crete, Greece, observed by an amphibian network. *J. Seismol.* **2010**, *14*, 369–392.
34. Lee, W.H.K.; Lahr, J.C. *HYP071 (Revised): A Computer Program for Determining Hypocenter, Magnitude, and First Motion Pattern of Local Earthquakes*; U.S. Geological Survey Open File Report 75-311; U.S. Geological Survey: Reston, VA, USA, 1975.
35. Klein, F.W. *User's Guide to HYPOINVERSE-2000, a Fortran Program to Solve for Earthquake Locations and Magnitudes, 2002–2171*; United States Department of The Interior Geological Survey: Menlo Park, CA, USA, 2002; p. 123.
36. Kissling, E.; Ellsworth, W.L.; Eberhart-Phillips, D.; Kradolfer, U. Initial Reference Models in Local Earthquake Tomography. *J. Geophys. Res.* **1994**, *99*, 19635–19646.
37. Chiarabba, C.; Frepoli, A. Minimum 1D velocity models in Central and Southern Italy: A contribution to better constrain hypocentral determination. *Annali di Geofisica* **1997**, *40*, 937–954. [CrossRef]
38. Mignan, A.; Chouliaras, G. Fifty Years of Seismic Network Performance in Greece (1964–2013): Spatiotemporal Evolution of the Completeness Magnitude. *Seismol. Res. Lett.* **2014**, *85*, 657–667. [CrossRef]
39. Nikolintaga, I.; Karakostas, V.; Papadimitriou, E.; Vallianatos, F. Velocity models inferred from P-waves travel time curves in South Aegean. *Bull. Geol. Soc. Greece* **2007**, *40*, 1187–1198.
40. Triantafyllou, I.; Karavias, A.; Koukouvelas, I.; Papadopoulos, G.A.; Parcharidis, I. The Crete Isl. (Greece) Mw6.0 Earthquake of 27 September 2021: Expecting the Unexpected. *GeoHazards* **2022**, *3*, 106–124. [CrossRef]
41. Ganas, A.; Hamiel, Y.; Serpetsidaki, A.; Briole, P.; Valkaniotis, S.; Fassoulas, C.; Piatibratova, O.; Kranis, H.; Tsironi, V.; Karamitros, I.; et al. The Arkalochori Mw = 5.9 Earthquake of 27 September 2021 Inside the Heraklion Basin: A Shallow, Blind Rupture Event Highlighting the Orthogonal Extension of Central Crete. *Geosciences* **2022**, *12*, 220. [CrossRef]
42. Chatelain, J.L. Etude Fine de la Sismicité en Zone de Collision Continentale au Moyen d'un Réseau de Stations Portables: La Région Hindu-Kush Pamir. Ph.D. Dissertation, Université Scientifique et Médicale de Grenoble, Grenoble, France, 1978.
43. Waldhauser, F. *hypoDD-A Program to Compute Double-Difference Hypocenter Locations, Open-File Report, 01-113*; U.S. Geological Survey: Menlo Park, CA, USA, 2001.
44. Spakman, W.; Nolet, G. Imaging algorithms, accuracy and resolution in delay time tomography. In *Mathematical Geophysics: A Survey of Recent Developments in Seismology and Geodynamics*; Vlaar, N.J., Nolet, G., Wortel, M.J.R., Cloetingh, S.A.P., Eds.; Springer: Berlin/Heidelberg, Germany, 1988; pp. 155–187.
45. Papazachos, B.C.; Nolet, G. P and S deep velocity structure of the Hellenic area obtained by robust non-linear inversion of arrival times. *J. Geophys. Res.* **1997**, *102*, 8349–8367.
46. Li, X.; Bock, G.; Vafidis, A.; Kind, R.; Harjes, H.P.; Hanka, W.; Wylegalla, K.; van der Meijde, M.; Yuan, X. Receiver function study of the Hellenic subduction zone: Imaging crustal thickness variations and the oceanic Moho of the descending African lithosphere. *Geophys. J. Int.* **2003**, *155*, 733–748.
47. Vallianatos, F.; Kokinou, E.; Sammonds, P. Non Extensive statistical physics approach to fault population distribution. A case study from the Southern Hellenic Arc (Central Crete). *Acta Geophys.* **2011**, *59*, 770–784.
48. Makris, J.; Yegorova, T. A 3-D density–velocity model between the Cretan Sea and Libya. *Tectonophysics* **2006**, *417*, 3–4, 201.
49. Kokinou, E.; Vallianatos, F. Seismic velocity Structure and Waveform Modelling in the southern Hellenic Arc (offshore Crete). In Proceedings of the 2nd IASME/WSEAS International Conference on Geology and Seismology (GES'08), Cambridge, UK, 23–25 February 2008.
50. Sachpazi, M.; Hirn, A.; Clément, C.; Haslinger, F.; Laigle, M.; Kissling, E.; Charvis, P.; Hello, Y.; Lépine, J.-C.; Sapin, M.; et al. Western Hellenic subduction and Cephalonia Transform: Local earthquakes and plate transport and strain. *Tectonophysics* **2000**, *319*, 301–319.
51. Ventouzi, C.; Papazachos, C.; Hatzidimitriou, P.; Papaioannou, C.; EGELADOS Working Group. Anelastic P- and S- upper mantle attenuation tomography of the southern Aegean Sea subduction area (Hellenic Arc) using intermediate-depth earthquake data. *Geophys. J. Int.* **2018**, *215*, 635–658. [CrossRef]
52. Sboras, S.; Pavlides, S.; Kilias, A.; Galanakis, D.; Chatziioannou, A.; Chatzipetros, A. The Geological Structure and Tectonic Complexity of Northern Thessaly That Hosted the March 2021 Seismic Crisis. *Geotechnics* **2022**, *2*, 935–960. [CrossRef]
53. Kokinou, E.; Alves, T.M.; Kamberis, E. Structural decoupling on a convergent forearc setting (Southern Crete, Eastern Mediterranean). *Geol. Soc. Am. Bull.* **2012**, *124*, 1352–1364.
54. Peacock, S.M. Are the lower planes of double seismic zones caused by serpentine dehydration in subducting oceanic mantle? *Geology* **2001**, *29*, 299–302.
55. Hacker, B.R.; Abers, G.A.; Peacock, S.M. Subduction factory 1. Theoretical mineralogy, densities, seismic wave speeds, and H_2O contents. *J. Geophys. Res. Solid Earth* **2003**, *108*, B1.
56. Hacker, B.R.; Peacock, S.M.; Abers, G.A.; Holloway, S.D. Subduction factory 2. Are intermediate-depth earthquakes in subducting slabs linked to metamorphic dehydration reactions? *J. Geophys. Res. Solid Earth* **2003**, *108*, B1.

57. Kato, A.; Iidaka, T.; Ikuta, R.; Yoshida, Y.; Katsumata, K.; Iwasaki, T.; Watanabe, T. Variations of fluid pressure within the subducting oceanic crust and slow earthquakes. *Geophys. Res. Lett.* **2010**, *37*, 14.
58. Pasten-Araya, F.; Salazar, P.; Ruiz, S.; Rivera, E.; Potin, B.; Maksymowicz, A.; Torres, E.; Villarroel, J.; Cruz, E.; Valenzuela, J.; et al. Fluids along the plate interface influencing the frictional regime of the Chilean Subduction zone, northern Chile. *Geophys. Res. Lett.* **2018**, *45*, 10378–10388. [CrossRef]
59. Husen, S.; Kissling, E. Postseismic fluid flow after the large subduction earthquake of Antofagasta, Chile. *Geology* **2001**, *29*, 847–850.
60. Barnes, P.M.; Lamarche, G.; Bialas, J.; Henrys, S.; Pecher, I.; Netzeband, G.L.; Crutchley, G. Tectonic and geological framework for gas hydrates and cold seeps on the Hikurangi subduction margin, New Zealand. *Mar. Geol.* **2010**, *272*, 26–48.
61. Collings, R.; Lange, D.; Rietbrock, A.; Tilmann, F.; Natawidjaja, D.; Suwargadi, B.; Saul, J. Structure and seismogenic properties of the Mentawai segment of the Sumatra subduction zone revealed by local earthquake traveltime tomography. *J. Geophys. Res. Solid Earth* **2012**, *117*, B1.
62. Bangs, N.L.; McIntosh, K.D.; Silver, E.A.; Kluesner, J.W.; Ranero, C.R. Fluid accumulation along the Costa Rica subduction thrust and development of the seismogenic zone. *J. Geophys. Res. Solid Earth* **2015**, *120*, 67–86.
63. Vallianatos, F.; Karakonstantis, A.; Michas, G.; Pavlou, K.; Kouli, M.; Sakkas, V. On the Patterns and Scaling Properties of the 2021–2022 Arkalochori Earthquake Sequence (Central Crete, Greece) Based on Seismological, Geophysical and Satellite Observations. *Appl. Sci.* **2022**, *12*, 7716. [CrossRef]
64. Delibasis, N.D.; Ziazia, M.; Voulgaris, N.; Papadopoulos, T.; Stavrakakis, G.N.; Papanastassiou, D.; Drakatos, G. Microseismic activity and seismotectonics of Heraklion Area (central Crete Island, Greece). *Tectonophysics* **1999**, *308*, 237–248. [CrossRef]
65. Famiglietti, N.A.; Golshadi, Z.; Vallianatos, F.; Caputo, R.; Kouli, M.; Sakkas, V.; Atzori, S.; Moschillo, R.; Cecere, G.; D'Ambrosio, C.; et al. The 2021 Greece Central Crete M_L 5.8 Earthquake: An Example of Coalescent Fault Segments Reconstructed from InSAR and GNSS Data. *Remote Sens.* **2022**, *14*, 5783. [CrossRef]
66. University of Athens. University of Athens. Hellenic Seismological Network, University of Athens, Seismological Laboratory [Data Set]. International Federation of Digital Seismograph Networks. 2008. Available online: https://www.fdsn.org/networks/detail/HA/ (accessed on 31 May 2023).
67. Aristotle University of Thessaloniki. Aristotle University of Thessaloniki Seismological Network [Data Set]. International Federation of Digital Seismograph Networks. 1981. Available online: https://www.fdsn.org/networks/detail/HT/ (accessed on 31 May 2023).
68. ITSAK. *Arkalochori Earthquakes, M 6.0 on 27/09/2021 & M 5.3 on 28/09/2021: Preliminary Report—Recordings of the ITSAK Accelerometric Network and Damage on the Natural and Built Environment*; ITSAK Research Unit: Thessaloniki, Greece, 2021; p. 44.
69. Hellenic Mediterranean University Research Center (Former Technological Educational Institute of Crete). *Seismological Network of Crete*; 10.7914/SN/HC; International Federation of Digital Seismograph Networks: Crete, Greece, 2006.